AN OBSTACLE IDENTIFICATION ALGORITHM FOR A LASER RANGE FINDER-BASED OBSTACLE DETECTOR

M. Kise, Q. Zhang, N. Noguchi

ABSTRACT. *The capability of detecting and identifying obstacles on the expected path and taking appropriate collision avoidance actions automatically is critical for safe operation of autonomous agricultural vehicles. This article presents an obstacle detection and identification algorithm for an on-tractor laser range finder-based obstacle detector. This algorithm consists of a template matching function and a Kalman filter for detecting the location of an obstacle, reconstructing the silhouette of the detected obstacle, and estimating its relative motions. Field validation test results verified that this obstacle detector was capable of detecting a moving object within a semicircle of 8 m radius and reconstructing a 2D silhouette of the obstacle progressively in real time. The errors of this obstacle detector in estimating the position, speed, and moving direction of the obstacle relative to the tractor were 0.052 m, 0.11 m* s^{-1}*, and 1.2°, respectively. Such accuracies are sufficient for providing safety warning and collision avoidance for autonomous tractors in field operation.*

Keywords. *Autonomous tractor, Collision avoidance, Kalman filter, Obstacle detection, Template matching, Tractor safety, Silhouette reconstruction.*

The efforts to develop automated or autonomous guidance systems for agricultural vehicles are motivated by the decrease in farming labor force and the desire for higher production efficiency and safer operations. Automated or autonomously guided agricultural vehicles can be operated faster with consistent performance. Automated guidance will also result in more accurate crop row tracking over time than a human operator achieves in long-hour field operations and will therefore enhance operation efficiency and productivity (Reid, 2000). Numerous successful research efforts on developing automated agricultural vehicle guidance technologies have been reported since late 1980s (Reid et al., 2000). In terms of the involvement of a human operator in maneuvering the vehicle, automated guidance systems can be roughly classified into operator-assistant systems and autonomous systems. An operator-assistant system uses an auto-track function to guide the vehicle, following crop rows automatically, and relies on a human operator to drive the vehicle to make end-row turns (Mizushima et al., 2002; Benson et al., 2003). An autonomous system can replace the human operator completely to implement all vehicle maneuvering functions automatically (Glasmacher, 2002). In both categories, GPS receivers are often used as either the principal or a complementary navigation sensor. For example, a tractor automated guidance system developed at Stanford University employed four RTK-GPS receivers to provide tractor posture information (Bell, 2000), and an integrated guidance system developed at Hokkaido University used an RTK-GPS to provide tractor position information and an IMU (inertial measurement unit) to provide tractor heading information (Kise et al., 2001).

Automated/autonomous agricultural vehicle creates a new challenge for operation safety. Although an autonomous agricultural vehicle improves operator safety by removing the human operator from the vehicle, it creates a safety concern without providing a safety watch to prevent collision with humans or other vehicles in the vicinity of the operating vehicle. Therefore, it is essential to furnish autonomous vehicles with some safety assurance means, including obstacle detection and collision avoidance, before autonomous vehicles can be deployed for commercial applications. Recently, some research efforts on developing safety assurance technologies for mobile equipment have been reported. Researchers have investigated the use of different types of obstacle detecting sensors, such as ultrasonic, radar, laser, and vision sensors (Guo et al., 2002; Kato et al., 2002; Fang et al., 2002; Aufrère et al., 2003), to detect obstacles and locate their position in relation to the operating vehicle.

To effectively prevent the operating vehicle from colliding with an obstacle, it is essential not only to locate the detected obstacle, but also to avoid a collision based on the assessment of the possibility of collision in terms of the relative motion between the vehicle and the detected obstacle. Research efforts on collision avoidance methods for mobile robots operating in controlled environments have been reported. Some successful examples include a multiple-robot collision avoidance function to coordinate the motion

Article was submitted for review in March 2004; approved for publication by the Information & Electrical Technologies Division of ASAE in April 2005.

The authors are **Michio Kise, ASAE Member,** Visiting Post-Doctoral Research Associate, **Qin Zhang, ASAE Member Engineer,** Associate Professor, Department of Agricultural and Biological Engineering, University of Illinois at Urbana-Champaign; and **Noboru Noguchi**, **ASAE Member Engineer,** Professor, Graduate School of Agriculture, Hokkaido University, Japan. **Corresponding author:** Qin Zhang, University of Illinois at Urbana-Champaign, 1304 W. Pennsylvania Ave., Urbana, IL 61801; phone: 217-333-9419; fax: 217-244-0323; e-mail: qinzhang@uiuc.edu.

  ISSN 0001−2351

of all robots operating on the same site (Yamashita et al., 2003) and a path planning function to guide an underwater robot to avoid the detected obstacle (Petillot et al., 2001). In both cases, the collision avoidance function was based on changing the path of the robot to avoid possible collision.

Multiple vehicles operating in the same field often cause a safety concern in farming operations. How to effectively detect the relative posture among these vehicles is essential for creating a practical collision avoidance method. Moreover, such posture generally only indicates the position and motion of the vehicle CG (center of gravity). It is also necessary to identify the shape of a detected object for reliable collision avoidance. The research reported here aimed to search for an effective method of obstacle detection and identification for autonomous agricultural vehicle. To accomplish this goal, a laser range finder-based obstacle detection system was developed. The core of this obstacle detection system is an obstacle detecting algorithm consisting of a template matching function and a Kalman filter for detecting the location of an obstacle, reconstructing the silhouette of the detected obstacle, and estimating its position and motion. The following sections describe the development of this algorithm, emphasizing the creation of the template matching function for detecting a moving obstacle and the Kalman filter for estimating the position and motion of the detected obstacle.

Obstacle Detection System Development

Obstacle Detection System

The obstacle detection system was developed based on an LMS291 laser range finder (SICK AG, Waldkirch, Germany). This laser range finder (LRF) employs a laser optical scanner to detect the distance of an object of interest by measuring the "time-of-flight" of laser light pulses. During the measurement, the scanner emits pulsed laser beams and receives the beams being reflected from a detected object. The distance of the detected object is determined by the time interval between the emission and reception of the laser beams. Other than distance measurements, the LRF can also be used to survey the 3D working environment for robots (Arras et al., 2001) and make non-contact replication of a sculpture (Fowles, 2000).

The developed obstacle detection system can horizontally scan a 180° arc of up to 8 m radius with 1° resolution (fig. 1). It takes 200 ms to complete a scan of 180°. The system will output a sequence of detected ranges (S^P) to locate the detected object in polar coordinates as follows:

$$S^P = \left\{ s_i^P = (\theta_i, d_i)^T \Big|_{s_i^P \in P}; i = 0, 1, \ldots, n_s; 0 \le n_s \le 180 \right\} \quad (1)$$

where θ_i and d_i are the angle and the distance in polar coordinates (P), and n_s is the number of data points being recorded.

Although the detection system provides a total of 181 data points in a complete scan, the detected range set (S^P) represents only the points on which the light beams are being reflected. Based on the recorded ranges (d_i) with associated measurement angles (θ_i), a silhouette of the detected object can be created.

To simplify the data processing, the recorded data in polar coordinates should be converted into Cartesian coordinates:

$$\begin{bmatrix} x_i^V \\ y_i^V \end{bmatrix} = \begin{bmatrix} d_i \cos\theta_i \\ d_i \sin\theta_i \end{bmatrix} \quad (2)$$

$$S^V = \{ s_i^V = (x_i^V, y_i^V)^T \Big|_{s_i^V \in V};\ i = 0,1, \ldots, n_s \} \quad (3)$$

where V is the sensor coordinates in Cartesian form, and $s_i^V = (x_i^V, y_i^V)^T$ represents the position data of the detected object in V coordinates.

The developed detection system was installed on the front bumper of a Kubota MD77 wheel-type agricultural tractor (Kubota, Sakai, Japan; called the "robot tractor" hereafter) about 0.6 m above the ground. This tractor was also equipped with an MS 750 RTK-GPS (Trimble, Sunnyvale, Cal.) and a JCS-7401A IMU (JAE, Tokyo, Japan) to measure its position, heading angle, and yaw rate.

Obstacle Detection Algorithm

A real-time obstacle detection algorithm is the core of this tractor obstacle detection system. As illustrated in figure 2, the obstacle detection algorithm consists of a template matching function, a template updating function, and a data fusion function. The template matching function was designed to represent the motion of a detected obstacle in sensor coordinates and to reconstruct the silhouette of the obstacle. The template matching function is the core function of this obstacle detection algorithm. The template updating func−

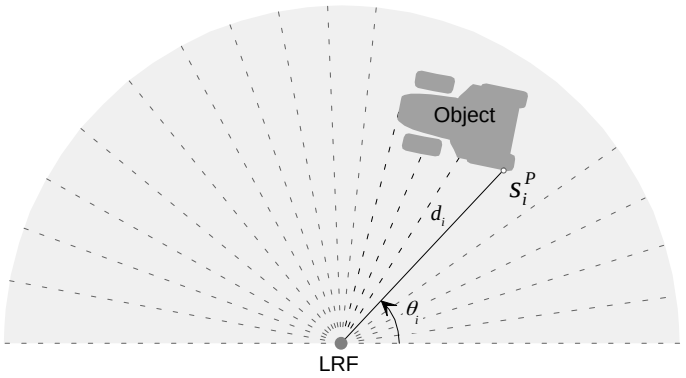

Figure 1. Principle of the sensor scanning for an object in its detectable area.

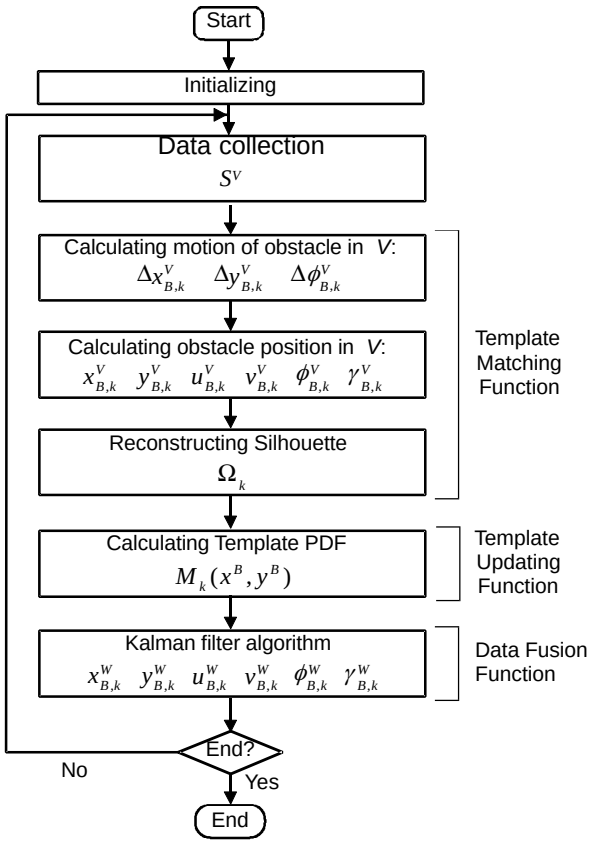

Figure 2. Flowchart of the obstacle detection algorithm (all parameters are described in the text).

tion was designed to update a probability density function of the detected obstacle. The data fusion function was designed to transform the obstacle position from sensor coordinates to global coordinates. This data fusion function uses a Kalman filter to combine the data obtained by the template matching with RTK-GPS and IMU readings obtained from the robot tractor to provide accurate obstacle dynamic position information.

Definition of Coordinate Systems

As mentioned earlier, the obstacle detection system uses three coordinate systems, namely the global coordinates (*W*), the sensor coordinates (*V*), and the obstacle coordinates (*B*), to determine the location of a detected obstacle. Figure 3 illustrates the definition and relationship of these coordinates. The half-circle gray area in figure 3 represents the region of sensor coordinates (*V*) because the detectable region of the LRF sensor is a half-circle in front of the robot tractor. The obstacle coordinates (*B*) are defined with respect to the center of the detected obstacle illustrated as point O_B in figure 3. It should be noted that coordinates *B* move on *V*, representing the relative motion of the detected obstacle within sensor detecting region. As shown in figure 3, $X^W_B = \left(x^W_B, y^W_B\right)^T$ and ϕ^W_B are defined as the position and the heading direction of the orientation point (O_B) of the obstacle coordinates (*B*) in global coordinates (*W*); $X^V_B = \left(x^V_B, y^V_B\right)^T$ and ϕ^V_B are defined as the position and the heading direction of O_B in sensor coordinates (*V*); and $X^W_V = \left(x^W_V, y^W_V\right)^T$ and ϕ^W_V are defined as the position and the heading direction of the origin point (O_V) of the sensor coordinates in global coordinates (*W*).

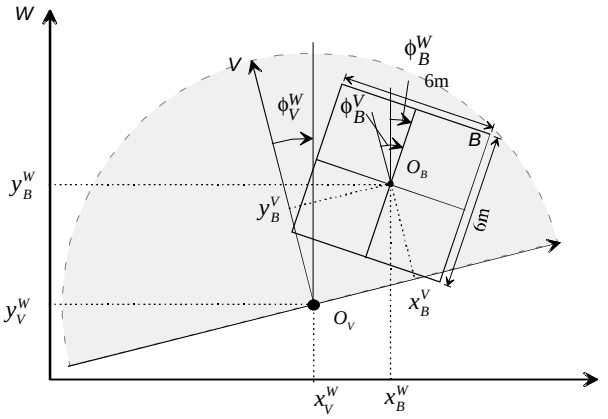

Figure 3. Definition of coordinates for the sensor-based obstacle detection system.

As defined in figure 3, the transform function between sensor coordinates and obstacle coordinates, $g_{VB}: V \to B$, can be derived based on their geometric relationship as follows:

$$X^B = g_{VB}\left(X^V\right) = J^{-1}\left(\phi^V_B\right)\left(X^V - X^V_B\right) \tag{4}$$

where X^V and X^B are position vectors in sensor and obstacle coordinates, respectively. $J(\phi)$ is the rotation matrix rotating a position vector (ϕ) clockwise about its origin, and is defined as:

$$J(\phi) = \begin{bmatrix} \cos\phi & \sin\phi \\ -\sin\phi & \cos\phi \end{bmatrix} \tag{5}$$

Similarly, the transform function from sensor to global coordinates, $g_{VW}: V \to W$, can be derived based on their geometric relationship to get a position vector (X^W) in global coordinates:

$$X^W = g_{VW}\left(X^V\right) = X^W_V + J\left(\phi^W_V\right)\left(X^V\right) \tag{6}$$

The heading directions of the defined coordinate systems in figure 3 satisfies the following relationship:

$$\phi^W_B = \phi^W_V + \phi^V_B \tag{7}$$

Determination of Obstacle Motion

The template matching function is designed to detect the motion of O_B, namely, the motion of the obstacle object in terms of translational and rotational motion in sensor coordinates:

$$\Delta x^V_{B,k} = x^V_{B,k} - x^V_{B,k-1} \tag{8}$$

$$\Delta y^V_{B,k} = y^V_{B,k} - y^V_{B,k-1} \tag{9}$$

$$\Delta \phi^V_{B,k} = \phi^V_{B,k} - \phi^V_{B,k-1} \tag{10}$$

where *k* represents the time step in the discrete-time system, and $\Delta X^V_{B,k} = \left(\Delta x^V_{B,k}, \Delta y^V_{B,k}\right)^T$ and $\Delta \phi^V_{B,k}$ are, respectively, the increments in translational and rotational motion of O_B from $k-1$ to *k* in *V* coordinates.

To determine the motion of an obstacle object, a template transform function (f) is defined based on measured $\Delta X^V_{B,k}$ and $\Delta\phi^V_{B,k}$ as follows:

$$X^V_k{}' = f_k\left(X^V_k\right) =$$

$$J\left(\Delta\phi^V_{B,k}\right)\left\{\left(X^V_k + \Delta X^V_{B,k}\right) - X^V_{B,k-1}\right\} + X^V_{B,k-1} \quad (11)$$

where X^V_k is an arbitrary vector in sensor coordinates obtained by the sensor at time instant k, hence representing one point on the edge of the detected obstacle object, and $X^V_k{}'$ is its projection, as shown in figure 4. This template transform represents the motion of the obstacle edge from k to $k-1$; thus, $X^V_k{}'$ and X^V_k must represent the same point on the edge of the detected obstacle.

Identification of Obstacle Silhouette

As described in the previous section, this system exploits the use of the template matching method for detecting an obstacle and tracking the detected obstacle in the field. As a basis of the template, a Ω_k data set holding the silhouette of the detected obstacle is defined in obstacle coordinates (B):

$$\Omega_k = \left\{\omega_{k,i} \,\middle|\, \omega_{k,i} = (p_i, q_i)^T, \omega_{k,i} \in B,\ i = 0,1, \ldots, n_{\omega,k} - 1\right\} \quad (12)$$

where $\omega_{k,i}$ is a position vector of a point on the edge of the detected obstacle object in B coordinates; thus, the Ω_k set represents an obstacle silhouette, and $n_{\omega,k}$ is the number of sensor data obtained from time 0 to k. The data provide the baseline data to define this set, and therefore Ω_k set is updated by the following equations:

$$S^V_k = \left\{s^V_{k,i} \,\middle|\, s^V_{k,i} \in V, i = 0, \ldots, n_{s,k} - 1\right\} \quad (13)$$

$$\Omega'_k = \left\{\omega'_{k,i} \,\middle|\, \omega'_{k,i} \in B, \omega'_{k,i} = g_{VB,k-1} \cdot f_k\left(s^V_{k,i}\right), i = 0,1, \ldots, n_{s,k} - 1\right\} \quad (14)$$

$$\Omega_k = \Omega_{k-1} + \Omega'_k \quad (15)$$

where S^V_k is the sensor data set at time instant k, $g_{VB,k-1}$ is the coordinates transform $V \rightarrow B$ at $k-1$, Ω'_k is the images of S^V_k under the composite transformation $g_{VB,k-1} \cdot f_k$, therefore, is the sensor data translated $-\Delta X^V_{B,k}$ and rotated $-\Delta\phi^V_{B,k}$ by f_k and then transformed from V coordinates to B coordinates by $g_{VB,k-1}$. Ω_k is updated by adding Ω'_k to Ω_{k-1} at every time step. A more complete silhouette of the detected obstacle is obtained with increasing time instant k since the number of the points of Ω_k increases progressively.

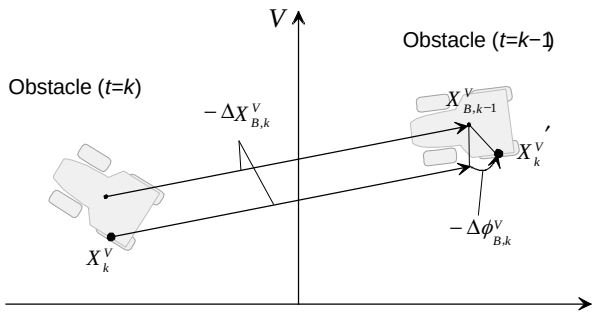

Figure 4. Geometry relationship of the transformation *f* (*f* transforms a detected point on the edge at time index *k* to *k*−1).

Template Probability Density Function

As discussed above, the motion of a detected obstacle is defined by ΔX^V_{Bk} and $\Delta\phi^V_{Bk}$. To determine ΔX^V_{Bk} and $\Delta\phi^V_{Bk}$, a template probability density function (TPDF), $M_k(x^B, y^B)$, is introduced. This TPDF represents the probability density function of the silhouette of the detected obstacle with reference to B coordinates using the following equation:

$$\mu_k(x^B, y^B) = \sum_{i=0}^{n_{\omega,k}-1} \frac{1}{\sqrt{2\pi}\sigma} \exp\left\{-\frac{\left(x^B - p_i\right)^2 + \left(y^B - q_i\right)^2}{2\sigma^2}\right\} \quad (16)$$

$$M_k(x^B, y^B) = \frac{\mu_k(x^B, y^B)}{\iint_B \mu_k(x, y)\,dx\,dy} \quad (17)$$

where $\mu_k(x^B, y^B)$ is an index representing the likelihood of an arbitrary point (x^B, y^B) being the edge of the detected obstacle, (p_i, q_i) is an element of Ω_k set defined by equation 12, $M_k(x^B, y^B)$ is a dimensionless value of $\mu_k(x^B, y^B)$, and σ is an empirical parameter dominating the shape of the normal distribution function in equation 16. The σ value was 0.06 determined experimentally in this research.

By applying the TPDF, a criteria function (I_k) can be defined as follows:

$$I_k = \sum_{i=0}^{n_{C,k}-1} M_{k-1}\left(\omega'_{k,i}\right) \quad (18)$$

where $\omega'_{k,i}$ is the element of Ω'_k set expressed by equation 14.

Equation 18 suggests that the maximum I_k represents the maximum overlapping Ω'_k with Ω_{k-1}. Replacing $\omega'_{k,i}$ using $s^V_{k,i}$, Δx^V_{Bk}, Δy^V_{Bk}, and $\Delta\phi^V_{Bk}$, this equation can be rewritten as follows:

$$I_k = \sum_{i=0}^{n_{Ck}-1} M_{k-1}\left(s^V_{k,i}, \Delta x^V_{B,k}, \Delta y^V_{B,k}, \Delta\phi^V_{B,k}\right) \quad (19)$$

Because I_k represents the degree of overlapping Ω'_k with Ω_{k-1}, optimal $\Delta\hat{x}^V_{Bk}$, $\Delta\hat{y}^V_{Bk}$, and $\Delta\hat{\phi}^V_{Bk}$ are obtained from the maximum I_k. Once the optimal $\Delta\hat{x}^V_{Bk}$, $\Delta\hat{y}^V_{Bk}$, and $\Delta\hat{\phi}^V_{Bk}$ are obtained, the position and heading angle of the detected obstacle in V coordinates can be calculated by substituting $\Delta\hat{x}^V_{Bk}$, $\Delta\hat{y}^V_{Bk}$, and $\Delta\hat{\phi}^V_{Bk}$ into equations 8 through 10 as follows:

$$x^V_{Bk} = x^V_{Bk-1} + \Delta\hat{x}^V_{Bk} \quad (20)$$

$$y^V_{Bk} = y^V_{Bk-1} + \Delta\hat{y}^V_{Bk} \quad (21)$$

$$\phi^V_{Bk} = \phi^V_{Bk-1} + \Delta\hat{\phi}^V_{Bk} \quad (22)$$

The speed and yaw rate of the detected obstacle can be determined using the following equations:

$$u_{Bk}^{V} = \frac{\Delta \hat{x}_{Bk}^{V}}{\Delta t} \quad (23)$$

$$v_{Bk}^{V} = \frac{\Delta \hat{y}_{Bk}^{V}}{\Delta t} \quad (24)$$

$$\gamma_{Bk}^{V} = \frac{\Delta \hat{\phi}_{Bk}^{V}}{\Delta t} \quad (25)$$

where Δt is the time interval, u_{Bk}^{V} and v_{Bk}^{V} are the horizontal and vertical direction components of the travel speed, and γ_{Bk}^{V} is the yaw rate.

KALMAN FILTER-BASED COORDINATES TRANSFORM

In this system, a Kalman filter was designed to transform the obstacle position from *V* coordinates to *W* coordinates by combining results of the template matching with RTK-GPS and IMU data. Because a Kalman filter can estimate a state of a linear system by using observation data online, this approach will not only transform the coordinates efficiently, but also enhance the accuracy of the obstacle position and motion detection. This Kalman filter-based coordinates transformation algorithm consists of a system equation and an observation equation represented by a linear discrete stochastic system as follows:

$$X_{k+1} = A_k X_k + G_k E_k \quad (26)$$

$$Y_k = H_k X_k + N_k \quad (27)$$

where X_k is an *n*th order state vector, Y_k a *p*th order observation vector, E_k an *r*th order process noise vector, and N_k is a *p*th order observation noise vector, respectively; A_k is an $n \times n$ state transition matrix, G_k an $n \times r$ driving matrix, and H_k a $p \times n$ observation matrix, respectively; and E_k and N_k are white noise vectors whose covariance matrixes (Q_k and R_k) are represented by:

$$E\left\{ \begin{bmatrix} E_k \\ N_k \end{bmatrix} \begin{bmatrix} E_l^T & N_l^T \end{bmatrix} \right\} = \begin{bmatrix} Q_k & 0 \\ 0 & R_k \end{bmatrix} \delta_i, \; R_k > 0 \quad (28)$$

where δ_{kl} is Kronecker delta.

The system equation of a detected obstacle can be defined based on the dynamics of a rigid body in terms of the status of the obstacle in the global coordinates (*W*). For an obstacle traveling as shown in figure 5, the system equation derived based on this method is given by:

$$\begin{bmatrix} x_{B\,k+1}^{W} \\ y_{B\,k+1}^{W} \\ u_{B\,k+1}^{W} \\ v_{B\,k+1}^{W} \\ \phi_{B\,k+1}^{W} \\ \gamma_{B\,k+1}^{W} \end{bmatrix} = \begin{bmatrix} 1 & 0 & \Delta t & 0 & 0 & 0 \\ 0 & 1 & 0 & \Delta t & 0 & 0 \\ 0 & 0 & 1 & 0 & 0 & 0 \\ 0 & 0 & 0 & 1 & 0 & 0 \\ 0 & 0 & 0 & 0 & 1 & \Delta t \\ 0 & 0 & 0 & 0 & 0 & 1 \end{bmatrix} \begin{bmatrix} x_{B\,k}^{W} \\ y_{B\,k}^{W} \\ u_{B\,k}^{W} \\ v_{B\,k}^{W} \\ \phi_{B\,k}^{W} \\ \gamma_{B\,k}^{W} \end{bmatrix} + \begin{bmatrix} \varepsilon_{xk} \\ \varepsilon_{y_k} \\ \varepsilon_{uk} \\ \varepsilon_{vk} \\ \varepsilon_{\phi k} \\ \varepsilon_{\gamma k} \end{bmatrix} \quad (29)$$

where Δt is the time interval, $\left(x_{B\,k}^{W}, y_{B\,k}^{W}\right)$ is the position, $u_{B\,k}^{W}$ and $v_{B\,k}^{W}$ are the horizontal and vertical speeds, $\phi_{B\,k}^{W}$ is the heading angle, $\gamma_{B\,k}^{W}$ is the yaw rate, and ε values are the process noises. This Kalman filter estimates the state vector representing the obstacle motion in *W* coordinates.

In this research, the data obtained by the template matching function include $\tilde{x}_{B\,k}^{V}$, $\tilde{y}_{B\,k}^{V}$, $\tilde{u}_{B\,k}^{V}$, $\tilde{v}_{B\,k}^{V}$, $\tilde{\phi}_{B\,k}^{V}$, and $\tilde{\gamma}_{B\,k}^{V}$. In addition, the RTK-GPS and IMU on the vehicle provided the information related to sensor position and motion, including the position $\left(\tilde{x}_{V\,k}^{W}, \tilde{y}_{V\,k}^{W}\right)$, the speed $\left(\tilde{u}_{V\,k}^{W}, \tilde{v}_{V\,k}^{W}\right)$, the heading angle $\left(\tilde{\phi}_{V\,k}^{W}\right)$, and the yaw rate $\left(\tilde{\gamma}_{V\,k}^{W}\right)$. Substituting both $\left(\tilde{x}_{B\,k}^{V} + \nu_{x_k}, \tilde{y}_{B\,k}^{V} + \nu_{y_k}\right)^T$ and $\left(\tilde{x}_{V\,k}^{W}, \tilde{y}_{V\,k}^{W}\right)^T$ into equation 6 and rearranging the equation resulted in the desired coordinates transform function:

$$J\left(\tilde{\phi}_{V\,k}^{W}\right) \begin{bmatrix} \tilde{x}_{B\,k}^{V} \\ \tilde{y}_{B\,k}^{V} \end{bmatrix} + \begin{bmatrix} \tilde{x}_{V\,k}^{W} \\ \tilde{y}_{V\,k}^{W} \end{bmatrix} = \begin{bmatrix} x_{B\,k}^{W} \\ y_{B\,k}^{W} \end{bmatrix} - J\left(\tilde{\phi}_{V\,k}^{W}\right) \begin{bmatrix} \nu_{x_k} \\ \nu_{y_k} \end{bmatrix} \quad (30)$$

where ν_{xk} and ν_{yk} are the observation noise related to $\tilde{x}_{B\,k}^{V}$ and $\tilde{y}_{B\,k}^{V}$.

It is noted that all observation variables are now represented in the left side of the equation, and state and noise variables are in the right side. To make it more understandable, equation 30 can be rewritten in a vector form as follows:

$$\begin{bmatrix} \tilde{y}_{xk} \\ \tilde{y}_{y_k} \end{bmatrix} = \begin{bmatrix} x_{B\,k}^{W} \\ y_{B\,k}^{W} \end{bmatrix} - J\left(\tilde{\phi}_{V\,k}^{W}\right) \begin{bmatrix} \nu_{xk} \\ \nu_{y_k} \end{bmatrix} \quad (31)$$

where $\begin{bmatrix} \tilde{y}_{xk} \\ \tilde{y}_{y_k} \end{bmatrix} = J\left(\tilde{\phi}_{V\,k}^{W}\right) \begin{bmatrix} \tilde{x}_{B\,k}^{V} \\ \tilde{y}_{B\,k}^{V} \end{bmatrix} + \begin{bmatrix} \tilde{x}_{V\,k}^{W} \\ \tilde{y}_{V\,k}^{W} \end{bmatrix}$.

The observation equation related to the travel speed of the robot tractor (and therefore the sensor) can be obtained by taking a time derivative on equation 6, resulting in the following equation:

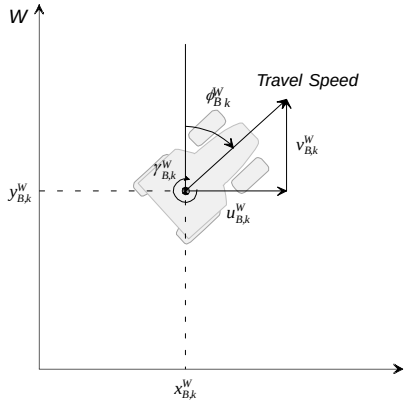

Figure 5. Status of the detected obstacle in global coordinates.

$$\frac{d}{dt}\left(g_{VW}\left(X^{V}\right)\right)=$$

$$\dot{X}_{V}^{W}+J\left(\phi_{V}^{W}\right)\left(\dot{X}^{V}\right)+\dot{J}\left(\phi_{V}^{W}\right)\left(X^{V}\right) \tag{32}$$

Substitute $\left(\tilde{u}_{V\,k}^{W},\tilde{v}_{V\,k}^{W}\right)^{T}$, $\tilde{\phi}_{V\,k}^{W}$, $\left(\tilde{u}_{B\,k}^{V}+\nu_{uk},\tilde{v}_{B\,k}^{V}+\nu_{vk}\right)^{T}$, $\left(\tilde{x}_{B\,k}^{V}+\nu_{xk},\tilde{y}_{B\,k}^{V}+\nu_{y_k}\right)^{T}$, and $\left(\tilde{x}_{V\,k}^{W},\tilde{y}_{V\,k}^{W}\right)^{T}$ into equation 32 and the resulting observation equation is in the following form:

$$\begin{bmatrix}u_{B\,k}^{W}\\ v_{B\,k}^{W}\end{bmatrix}=$$

$$\begin{bmatrix}\tilde{u}_{V\,k}^{W}\\ \tilde{v}_{V\,k}^{W}\end{bmatrix}+J\left(\tilde{\phi}_{V\,k}^{W}\right)\begin{bmatrix}\tilde{u}_{B\,k}^{V}+\nu_{uk}\\ \tilde{v}_{B\,k}^{V}+\nu_{vk}\end{bmatrix}+\dot{J}\left(\tilde{\phi}_{V\,k}^{W}\right)\begin{bmatrix}\tilde{x}_{B\,k}^{V}+\nu_{xk}\\ \tilde{y}_{B\,k}^{V}+\nu_{y_k}\end{bmatrix} \tag{33}$$

Because ν_{uk} and ν_{vk} are the observation noise related to $\tilde{u}_{B\,k}^{V}$ and $\tilde{v}_{B\,k}^{V}$, equation 33 can be rewritten as follows:

$$\begin{bmatrix}\tilde{u}_{V\,k}^{W}\\ \tilde{v}_{V\,k}^{W}\end{bmatrix}+\dot{J}\left(\tilde{\phi}_{V\,k}^{W}\right)\begin{bmatrix}\tilde{x}_{B\,k}^{V}\\ \tilde{y}_{B\,k}^{V}\end{bmatrix}+J\left(\tilde{\phi}_{V\,k}^{W}\right)\begin{bmatrix}\tilde{u}_{B\,k}^{V}\\ \tilde{v}_{B\,k}^{V}\end{bmatrix}=$$

$$\begin{bmatrix}u_{B\,k}^{W}\\ v_{B\,k}^{W}\end{bmatrix}-\left[\dot{J}\left(\tilde{\phi}_{V\,k}^{W}\right),J\left(\tilde{\phi}_{V\,k}^{W}\right)\right]\begin{bmatrix}\nu_{xk}\\ \nu_{y_k}\\ \nu_{uk}\\ \nu_{vk}\end{bmatrix} \tag{34}$$

where

$$\left[\dot{J}\left(\tilde{\phi}_{V\,k}^{W}\right),J\left(\tilde{\phi}_{V\,k}^{W}\right)\right]=$$

$$\begin{bmatrix}-\tilde{\gamma}_{V\,k}^{W}\sin\tilde{\phi}_{V\,k}^{W} & \tilde{\gamma}_{V\,k}^{W}\cos\tilde{\phi}_{V\,k}^{W} & \cos\tilde{\phi}_{V\,k}^{W} & \sin\tilde{\phi}_{V\,k}^{W}\\ -\tilde{\gamma}_{V\,k}^{W}\cos\tilde{\phi}_{V\,k}^{W} & -\tilde{\gamma}_{V\,k}^{W}\sin\tilde{\phi}_{V\,k}^{W} & -\sin\tilde{\phi}_{V\,k}^{W} & \cos\tilde{\phi}_{V\,k}^{W}\end{bmatrix}$$

Similar to equation 31, equation 34 can also be represented as a vector in the following form:

$$\begin{bmatrix}\tilde{y}_{uk}\\ \tilde{y}_{vk}\end{bmatrix}=\begin{bmatrix}u_{B\,k}^{W}\\ v_{B\,k}^{W}\end{bmatrix}-\left[\dot{J}\left(\tilde{\phi}_{V\,k}^{W}\right),J\left(\tilde{\phi}_{V\,k}^{W}\right)\right]\begin{bmatrix}\nu_{xk}\\ \nu_{y_k}\\ \nu_{uk}\\ \nu_{vk}\end{bmatrix} \tag{35}$$

where $\begin{bmatrix}\tilde{y}_{uk}\\ \tilde{y}_{vk}\end{bmatrix}=\begin{bmatrix}\tilde{u}_{V\,k}^{W}\\ \tilde{v}_{V\,k}^{W}\end{bmatrix}+\dot{J}\left(\tilde{\phi}_{V\,k}^{W}\right)\begin{bmatrix}\tilde{x}_{B\,k}^{V}\\ \tilde{y}_{B\,k}^{V}\end{bmatrix}+J\left(\tilde{\phi}_{V\,k}^{W}\right)\begin{bmatrix}\tilde{u}_{B\,k}^{V}\\ \tilde{v}_{B\,k}^{V}\end{bmatrix}$.

The observation equation related to the heading angle can be obtained by substituting $\tilde{\phi}_{B\,k}^{V}+\nu_{\phi_k}$ and $\tilde{\phi}_{V\,k}^{W}$ into equation 7 as follows:

$$\tilde{\phi}_{V\,k}^{W}+\tilde{\phi}_{B\,k}^{V}=\phi_{B\,k}^{W}+\nu_{\phi_k} \tag{36}$$

where ν_{ϕ_k} is the observation noise related to $\tilde{\phi}_{B\,k}^{V}$. Similar to equation 31 and 35, the left side of equation 36 can be represented by:

$$\tilde{y}_{\phi_k}=\phi_{B\,k}^{W}+\nu_{\phi_k} \tag{37}$$

where $\tilde{y}_{\phi_k}=\tilde{\phi}_{V\,k}^{W}+\tilde{\phi}_{B\,k}^{V}$.

Similarly, taking a time derivative on equation 7 and substituting $\tilde{\gamma}_{B\,k}^{V}+\nu_{\gamma_k}$ and $\tilde{\gamma}_{V\,k}^{W}$ into the derived equation results in the following equation:

$$\tilde{y}_{\gamma_k}=\gamma_{B\,k}^{W}-\nu_{\gamma_k} \tag{38}$$

where $\tilde{y}_{\gamma_k}=\tilde{\gamma}_{B\,k}^{V}+\tilde{\gamma}_{V\,k}^{W}$.

Integrating equations 31, 35, 37, and 38 results in the observation equation of the Kalman filter as follows:

$$\begin{bmatrix}\tilde{y}_{xk}\\ \tilde{y}_{y_k}\\ \tilde{y}_{uk}\\ \tilde{y}_{vk}\\ \tilde{y}_{\phi_k}\\ \tilde{y}_{\gamma_k}\end{bmatrix}=\begin{bmatrix}x_{B\,k}^{W}\\ y_{B\,k}^{W}\\ u_{B\,k}^{W}\\ v_{B\,k}^{W}\\ \phi_{B\,k}^{W}\\ \gamma_{B\,k}^{W}\end{bmatrix}-\begin{bmatrix}J\left(\tilde{\phi}_{V\,k}^{W}\right) & 0 & 0\\ \dot{J}\left(\tilde{\phi}_{V\,k}^{W}\right) & J\left(\tilde{\phi}_{V\,k}^{W}\right) & 0\\ 0 & 0 & I\end{bmatrix}\begin{bmatrix}\nu_{xk}\\ \nu_{y_k}\\ \nu_{uk}\\ \nu_{vk}\\ \nu_{\phi_k}\\ \nu_{\gamma_k}\end{bmatrix} \tag{39}$$

where I is a 2×2 unit matrix. Equation 39 can be represented in matrix form:

$$Y_{k}'=X_{k}-D_{k}N_{k} \tag{40}$$

Defining $Y_{k}=-D_{k}^{-1}Y_{k}'$ and $H_{k}=-D_{k}^{-1}$, the observation equation can be rewritten as follows:

$$Y_{k}=H_{k}X_{k}+N_{k} \tag{41}$$

where

$$H_{k}=\begin{bmatrix}-\cos\tilde{\phi}_{V\,k}^{W} & \sin\tilde{\phi}_{V\,k}^{W} & 0 & 0 & 0 & 0\\ -\sin\tilde{\phi}_{V\,k}^{W} & -\cos\tilde{\phi}_{V\,k}^{W} & 0 & 0 & 0 & 0\\ \tilde{\gamma}_{V\,k}^{W}\sin\tilde{\phi}_{V\,k}^{W} & \tilde{\gamma}_{V\,k}^{W}\cos\tilde{\phi}_{V\,k}^{W} & -\cos\tilde{\phi}_{V\,k}^{W} & \sin\tilde{\phi}_{V\,k}^{W} & 0 & 0\\ -\tilde{\gamma}_{V\,k}^{W}\cos\tilde{\phi}_{V\,k}^{W} & \tilde{\gamma}_{V\,k}^{W}\sin\tilde{\phi}_{V\,k}^{W} & -\sin\tilde{\phi}_{V\,k}^{W} & -\cos\tilde{\phi}_{V\,k}^{W} & 0 & 0\\ 0 & 0 & 0 & 0 & -1 & 0\\ 0 & 0 & 0 & 0 & 0 & -1\end{bmatrix}$$

$$Y_{k}=-\begin{bmatrix}\tilde{x}_{B\,k}^{V}\\ \tilde{y}_{B\,k}^{V}\\ \tilde{u}_{B\,k}^{V}\\ \tilde{v}_{B\,k}^{V}\\ \tilde{\phi}_{B\,k}^{V}\\ \tilde{\gamma}_{B\,k}^{V}\end{bmatrix}+H_{k}\begin{bmatrix}\tilde{x}_{V\,k}^{W}\\ \tilde{y}_{V\,k}^{W}\\ \tilde{u}_{V\,k}^{W}\\ \tilde{v}_{V\,k}^{W}\\ \tilde{\phi}_{V\,k}^{W}\\ \tilde{\gamma}_{V\,k}^{W}\end{bmatrix}$$

After the system equation and the observation equation are defined, the Kalman filter for the obstacle detection system can be expressed as follows:

$$\hat{X}_{k+1/k}=A\hat{X}_{k/k} \tag{42}$$

$$\hat{X}_{k/k}=\hat{X}_{k/k-1}+K_{k}\left[Y_{k}-H_{k}\hat{X}_{k/k-1}\right] \tag{43}$$

$$K_k = P_{k/k-1} H_k^T \left[H_k P_{k/k-1} H_k^T + R \right]^{-1} \quad (44)$$

$$P_{k+1/k} = A P_{k/k} A^T + Q \quad (45)$$

$$P_{k/k} = P_{k/k-1} - K_k H_k P_{k/k-1} \quad (46)$$

where $\hat{X}_{k/k}$ is the state vector estimated using the Kalman filter at time instant k, K_k the Kalman gain, and P_k the covariance matrix of predict error. Q and R are the covariance matrices of noise vectors expressed by equation 28, and are empirically identified as follows:

$$Q = \begin{bmatrix} 0.01 & 0 & 0 & 0 & 0 & 0 \\ 0 & 0.01 & 0 & 0 & 0 & 0 \\ 0 & 0 & 1.0 & 0 & 0 & 0 \\ 0 & 0 & 0 & 1.0 & 0 & 0 \\ 0 & 0 & 0 & 0 & 3.49 \cdot 10^{-3} & 0 \\ 0 & 0 & 0 & 0 & 0 & 3.49 \cdot 10^{-3} \end{bmatrix} \quad (47)$$

$$R = \begin{bmatrix} 0.05 & 0 & 0 & 0 & 0 & 0 \\ 0 & 0.05 & 0 & 0 & 0 & 0 \\ 0 & 0 & 0.25 & 0 & 0 & 0 \\ 0 & 0 & 0 & 0.25 & 0 & 0 \\ 0 & 0 & 0 & 0 & 0.17 & 0 \\ 0 & 0 & 0 & 0 & 0 & 0.052 \end{bmatrix} \quad (48)$$

Calculating equations 42 through 46 recursively, the state vector can accurately estimate the position, heading, yaw rate, and the speed of the detected obstacle in W coordinates.

Experimental Methods

To validate the capability of the developed system in detecting obstacles in the field, another Kubota tractor (model GL 320) was modified as a moving obstacle in the field (called the "obstacle tractor" hereafter). This obstacle tractor was also equipped with an RTK-GPS and an IMU for providing its position and heading information as reference data to assess the accuracy of the estimated motion of the obstacle by the obstacle detection system. The RTK-GPS and the IMU provided a position accuracy of 0.02 m and a heading accuracy of 0.1° for the obstacle tractor in 10 Hz.

The validation tests were conducted at a research plot at Hokkaido University (Sapporo, Japan) where no other obstacle was presented in the vicinity of the robot tractor. As illustrated in figure 6, five types of field tests were defined to validate the capability of the developed system in detecting the obstacle tractor in different conditions. In a type I test, the robot tractor was parked in the field while the obstacle tractor was passing in front of the robot tractor. In a type II test, both the robot tractor and the obstacle tractor were moving on perpendicular paths, with the obstacle tractor passing in front of the moving robot tractor. In a type III test, the robot and the obstacle tractors were traveling in the same direction, with the robot tractor passing the obstacle tractor on the right side. In a type IV test, the robot tractor traveled toward the parked obstacle tractor. In a type V test, the robot tractor followed the obstacle tractor at the same speed. In all these field tests, the speed of moving tractors was between 0.8 and 1.1 m s^{-1}.

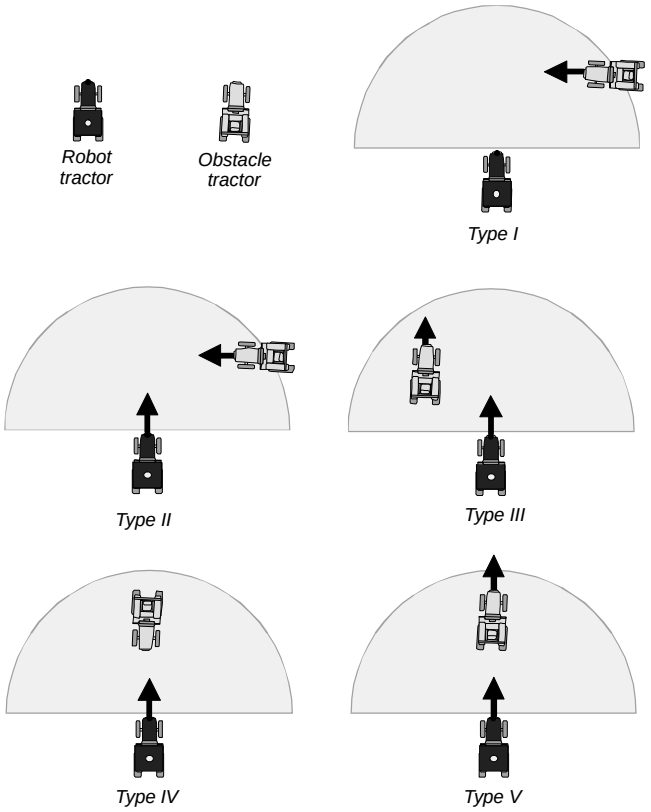

Figure 6. Definition of the types of validation tests: type I, obstacle tractor passing across in front of the stopped robot tractor; type II, obstacle tractor passing across in front of the moving robot tractor; type III, robot tractor passing the moving obstacle tractor on the side; type IV, robot tractor traveling toward the stopped obstacle tractor; and type V, robot tractor following the moving obstacle tractor.

Results and Discussion

As described previously, the ability of the developed obstacle detection system to track the motion of an obstacle was assessed using reference sensors, an RTK-GPS, and an IMU mounted on the obstacle tractor. The readings from these reference sensors were synchronized with the estimated motion of the detected obstacle using the global time provided by the RTK-GPS. Figure 7 shows the raw LRF sensor readings in the sensor coordinates (the V coordinates) obtained from one run in a type I test. This raw data indicates that it is very difficult to visually identify the object directly. Such a silhouette can be improved progressively by repeatedly scanning the object. Figure 8 illustrated the process of progressive silhouette reconstruction of the obstacle based on the sensed data sets as expressed by equation 12. During this silhouette reconstruction process, a total of 68 raw data sets were recorded over time and used to improve the recognizability of this silhouette progressively. As can be seen from this figure, it is hard to recognize that the detected obstacle is a tractor from the resulting silhouette using the first 20 data sets (fig. 8a with time instant k = 20). As the number of the data sets increased to 40 (fig. 8b), a front wheel and a rear wheel on the left side of the tractor start to be recognizable. After the silhouette was progressively reconstructed using all 68 recorded data sets, the resulting silhouette consists of the left side front and rear wheels, as well as the right side rear wheel (fig. 8c) because both the left and rear views of the obstacle tractor have been scanned during the process. A

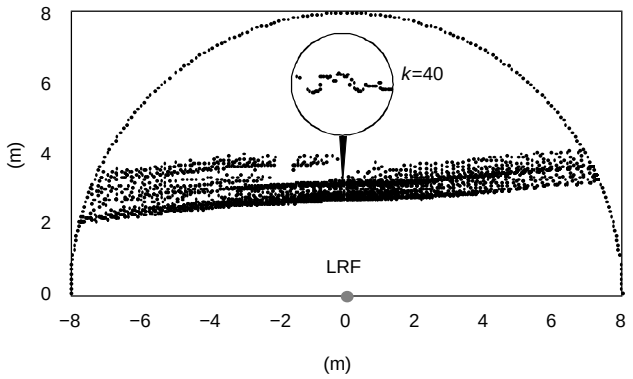

Figure 7. Raw sensor data obtained from a type I test: An instant data set recorded at time index k = 40 is shown in the circle.

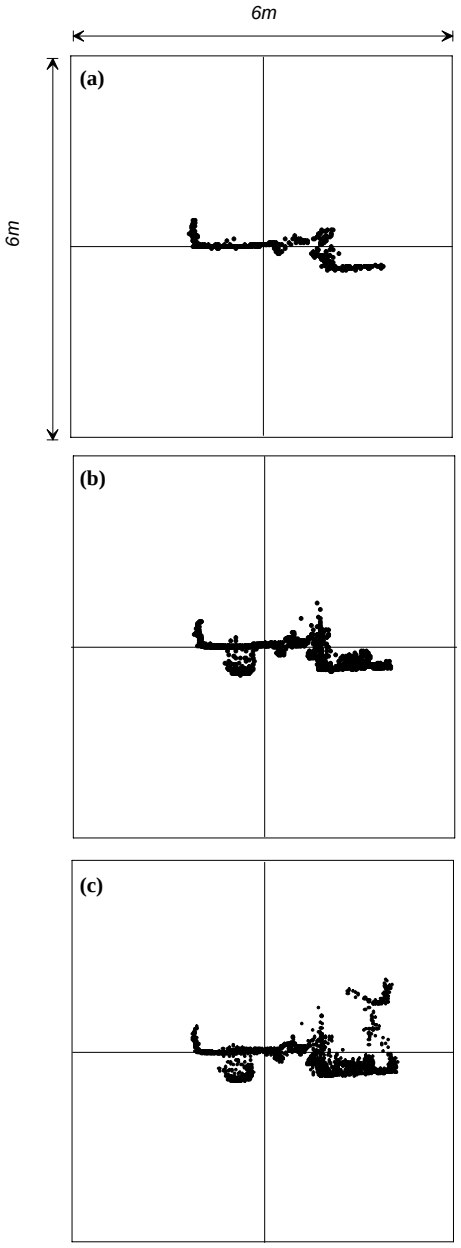

Figure 8. Progressive reconstruction of a 2D silhouette of the obstacle based on the template matching function: (a) the silhouette at time instant k = 20, (b) the silhouette at k = 47, and (c) the silhouette formed by 68 data sets.

multi-side view leads to much easier visual recognition of the detected obstacle. This silhouette reconstruction method furnishes the obstacle detection system with an excellent capability for automatic obstacle identification.

Figure 9 presents the errors in estimating the position, heading angle, and speed of the obstacle tractor as compared to the reference values obtained from one run of a type I test. In this particular test, a total of 68 data sets were recorded while the robot tractor was traveling at a speed between 0.8 and 1.1 m s^{-1}. Quantitative analysis of the obtained data sets revealed that the maximum error was 0.10 m in position detection, 3.0° in heading angle detection, and 0.3 m s^{-1} in speed detection. The root mean square (RMS) errors were 0.07 m, 1.7°, and 0.1 m s^{-1} for position, heading angle, and speed, respectively. The results indicated that the LRF-based detection system could reliably detect a moving obstacle tractor while the robot tractor was not in motion. The shaded area in figure 9 represents the missing data. However, the results showed that a Kalman filter was capable of estimating the motion status even when some data are missing.

The type II validation tests were designed to evaluate the performance of the developed system in detecting an obstacle tractor traveling in front of a moving robot tractor. Figure 10 presents the errors in estimating the position, heading angle, and speed of the obstacle tractor. In this test, the robot tractor was traveling at a speed varying between 0.8 and 1.1 m s^{-1},

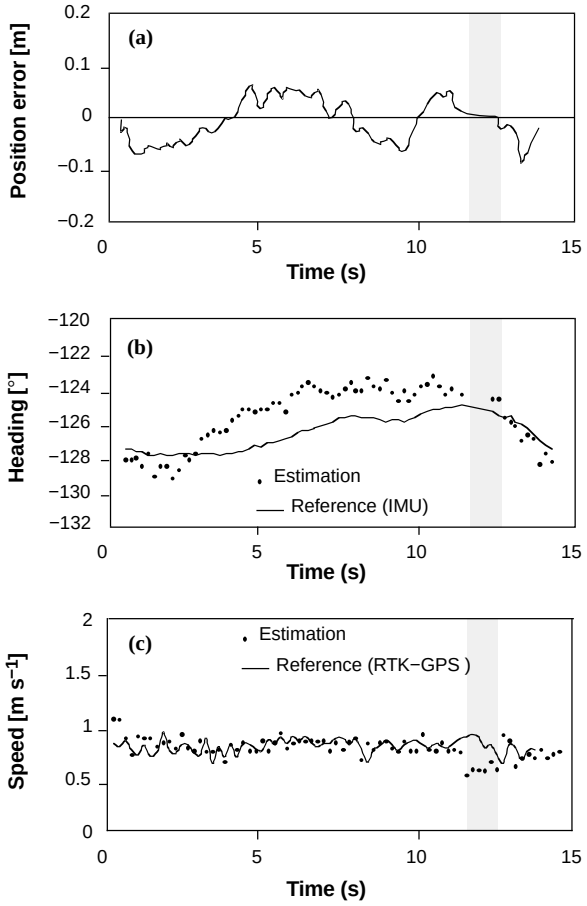

Figure 9. Errors from a type I test: (a) detected position errors compared with RTK-GPS readings, (b) estimated heading angle compared with IMU readings, and (c) estimated speed compared with RTK-GPS readings. The gray area around 12s indicates the duration of an unexpected LRF reading loss.

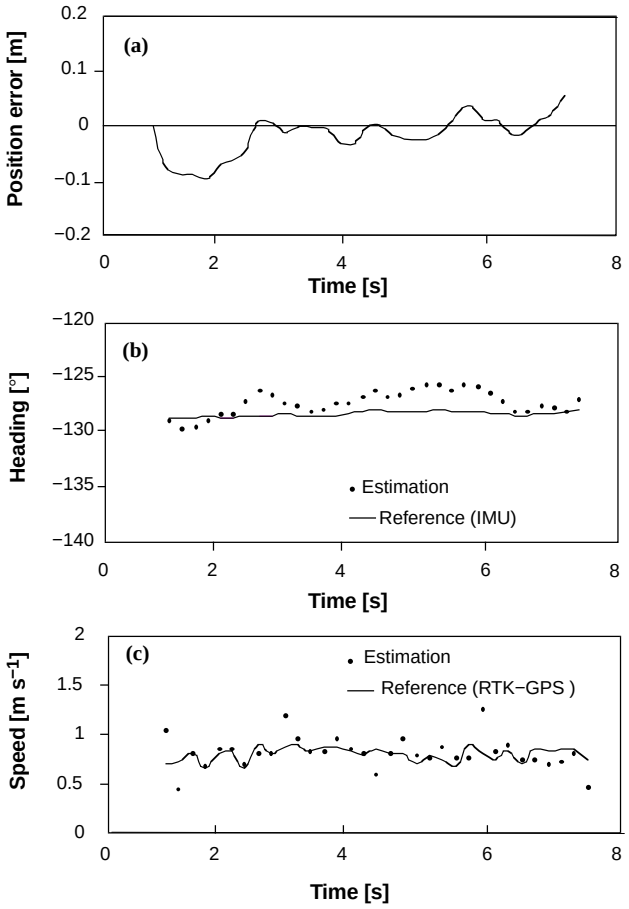

Figure 10. Errors from a type II test: (a) detected position errors compared with RTK-GPS readings, (b) estimated heading angle compared with IMU readings, and (c) estimated speed compared with RTK-GPS readings.

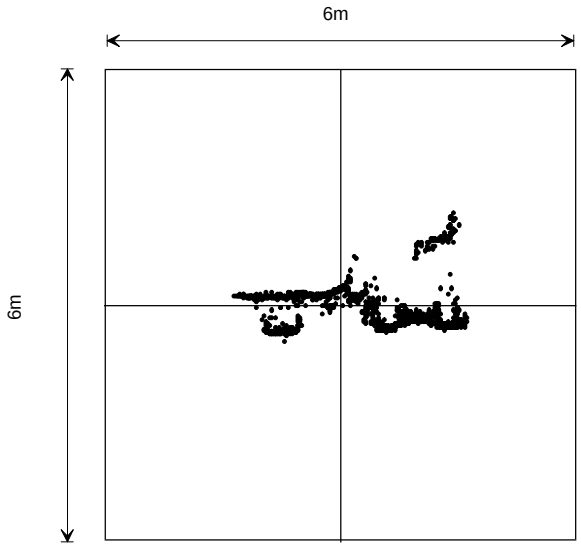

Figure 11. Final silhouette of the detected obstacle reconstructed based on 42 sets of data obtained from a type II test.

and the obstacle tractor was traveling at a speed varying between 0.4 and 0.7 m s^{-1}. A series of 42 data sets was obtained from this particular run of the type II test. Figure 11 shows the final silhouette from the progressive reconstruction. This result validated that the developed template matching function could reconstruct the silhouette of the detected obstacle from a moving robot tractor. Quantitative analysis of the results obtained from this test showed that the maximum estimation errors were 0.09 m, 2.6°, and 0.4 m s^{-1} for obstacle position, heading angle, and speed detection, respectively. The RMS errors for these components were 0.06 m, 1.4°, and 0.2 m s^{-1}, respectively. The results indicated that the LRF-based obstacle detection system could reliably detect an obstacle and accurately estimate the motion status of the obstacle from a moving robot tractor.

Table 1. Summary of error analysis on estimated motion variables of the detected obstacle from the five types of field tests.

Test Type	Position Error (m)		Heading Error (°)		Speed Error (m s^{-1})		No. of Data Sets
	Max.	RMS	Max.	RMS	Max.	RMS	
I	0.10	0.07	3.0	1.7	0.30	0.10	68
II	0.07	0.06	2.6	1.4	0.40	0.20	42
III	0.10	0.03	3.1	0.9	0.50	0. 07	420
IV	0.12	0.06	2.8	1.2	0.30	0. 12	50
V	0.15	0.04	3.0	0.9	0.40	0. 08	312
Avg	0.108	0.052	2.9	1.2	0. 38	0. 11	178

Numerous tests were conducted under all defined test conditions. Table 1 summarizes the performance of the obstacle detection system in estimating the motion variables of the obstacle from the five types of field validation tests. These results verify that the obstacle detection system can track the motion of the obstacle reliably from a platform either at rest or in motion. The tracking accuracy is independent of the relative position and motion of the obstacle. The average RMS errors under all test conditions were 0.052 m for positioning, 1.2° for heading, and 0.11 m s^{-1} for speed.

The results obtained from the validation tests proved that the developed system could provide a reliable obstacle detecting function for a robot tractor. In addition to detecting the motion status of an obstacle, this system can also identify the shape of the detected obstacle by reconstructing the silhouette of the obstacle progressively. Such information can provide much more complete information for creating a safer environment for agricultural operations using automated or autonomous vehicles.

CONCLUSION

Aimed at developing an effective obstacle detection system for automated and/or autonomous agricultural vehicle to ensure safe operations in the field, this research investigated the basic technology of sensor-based obstacle detection for robot tractors. A laser range finder-based obstacle detection system has been successfully developed. Results obtained from field validation tests indicate that this sensor-based obstacle detection system could reliably detect the motion status of the obstacle. The average root mean square (RMS) errors for estimating obstacle motion variables under five different test conditions were 0.052 m for position, 1.2° for heading, 0.11 m s^{-1} for speed. The results obtained from this investigation verified that it was possible to use a laser range finder to detect obstacles within the vicinity of operating agricultural vehicles to ensure safe operations.

As the main outcome from this investigation, the template matching function can progressively reconstruct the sil-

houette of the detected obstacle by updating the probability density function of the object in the obstacle template. Integrating this silhouette reconstruction function with an automatic pattern recognition algorithm, it is possible to form a complete obstacle avoidance system for robot agricultural tractors to detect and identify obstacles in their operating field, and to avoid possible collision with the detected obstacle if its shape and motion are known.

ACKNOWLEDGEMENTS

The material presented in this article was based upon work supported partially by the Graduate School of Agriculture at Hokkaido University, the Illinois Council on Food and Agricultural Research (IDA CF 99 SI-36-1A), and USDA Hatch Funds (ILLU-10-352 AE). The Japan Society for the Promotion of Science (JSPS) provides a Fellowship Fund to support Dr. Michio Kise's post-doctoral research at the University of Illinois at Urbana-Champaign. Any opinions, findings, and conclusions expressed in this publication are those of the authors and do not necessarily reflect the views of the University of Illinois, Hokkaido University, JSPS, Illinois CFAR, and USDA.

REFERENCES

Aufrère, R., J. Gowdy, C. Mertz, C. Thorpe, C. C. Wang, and T. Yata. 2003. Perception for collision avoidance and autonomous driving. *Mechatronics* 13(10): 1149-1161.

Arras, K. O., N. Tomatis, B. T. Jensen, and R. Siegwart. 2001. Multisensor on-the-fly localization: Precision and reliability for applications. *Robotics and Autonomous Systems* 34(2-3): 131-143.

Bell, T. 2000. Automatic tractor guidance using carrier-phase differential GPS. *Computer and Electronics in Agric.* 25(1-2): 53-66.

Benson, E. R., J. F. Reid, and Q. Zhang. 2003. Machine vision-based guidance system for an agricultural small-grain harvester. *Trans. ASAE* 46(4): 1255-1264.

Fang, Y., I. Masaki, and B. Horn. 2002. Depth-based target segmentation for intelligent vehicles: Fusion of radar and binocular stereo. *IEEE Trans. Intelligent Transportation Systems* 3(3): 196-202.

Fowles, P. S. 2000. The garden temple at Ince Blundell: A case study in the recording and non-contact replication of decayed sculpture. *J. Cult. Heritage* 1(1): 89-91.

Glasmacher, H. 2002. AGRO NAV Plan: Software for planning and evaluation of the path and work of field robots. In *Proc. Automation Technology for Off-Road Equipment*, 405-411. St. Joseph, Mich.: ASAE.

Guo, L., Q. Zhang, and S. Han. 2002. Agricultural machinery safety alert system using ultrasonic sensors. *J. Agric. Safety and Health* 8(4): 385-396.

Kato, T., Y. Ninomiya, and I. Masaki. 2002. An obstacle detection method by fusion of radar and motion stereo. *IEEE Trans. Intelligent Transportation Systems* 3(3): 182-188.

Kise, M., N. Noguchi, K. Ishii, and H. Terao. 2001. Development of agricultural autonomous tractor with an RTK-GPS and a FOG. *Proc. Fourth IFAC Symposium on Intelligent Autonomous Vehicles*, 103-106. Amsterdam, The Netherlands: Elsevier Science.

Mizushima, A., N. Noguchi, K. Ishii, and H. Terao. 2002. Automatic navigation of the agricultural vehicle by the geomagnetic direction sensor and gyroscope. *Proc. Automation Technology for Off-Road Equipment*, 204-211. St. Joseph, Mich.: ASAE.

Petillot, Y., I. T. Ruiz, and D. M. Lane. 2001. Underwater vehicle obstacle avoidance and path planning using a multi-beam forward looking sonar. *J . Oceanic Eng.* 26(2): 240-251.

Reid, J. F., Q. Zhang, N. Noguchi, and M. Dickson. 2000. Agricultural automatic guidance research in North America. *Computer and Electronics in Agric.* 25(1-2): 155-167.

Reid, J. F. 2000. Establishing automated vehicle navigation as a reality for production agriculture. *Proc. 2nd IFAC/CIGR International Workshop on Bio-robotics, Information Technology, and Intelligent Control for Bio* Production Systems, 22-26. Amsterdam, The Netherlands: Elsevier Science.

Yamashita, A., T. Arai, J. Ota, and H. Asama. 2003. Motion planning of multiple mobile robots for cooperative manipulation and transportation. *IEEE Trans. Robotics and Automation* 19(2): 223-237.